PNAS
www.pnas.org

Supplementary Information for
Topographic map formation and the effects of NMDA receptor blockade in the developing Xenopus retinotectal system

Vanessa J. Li[1], Anne Schohl[1], Edward S. Ruthazer[1]

[1]Montreal Neurological Institute-Hospital
Department of Neurology and Neurosurgery,
McGill University,
3801 Rue University,
Montréal, QC H3A 2B4, Canada

*Correspondence to: Edward S. Ruthazer
Email: edward.ruthazer@mcgill.ca

This PDF file includes:

Other supplementary materials for this manuscript include the following:

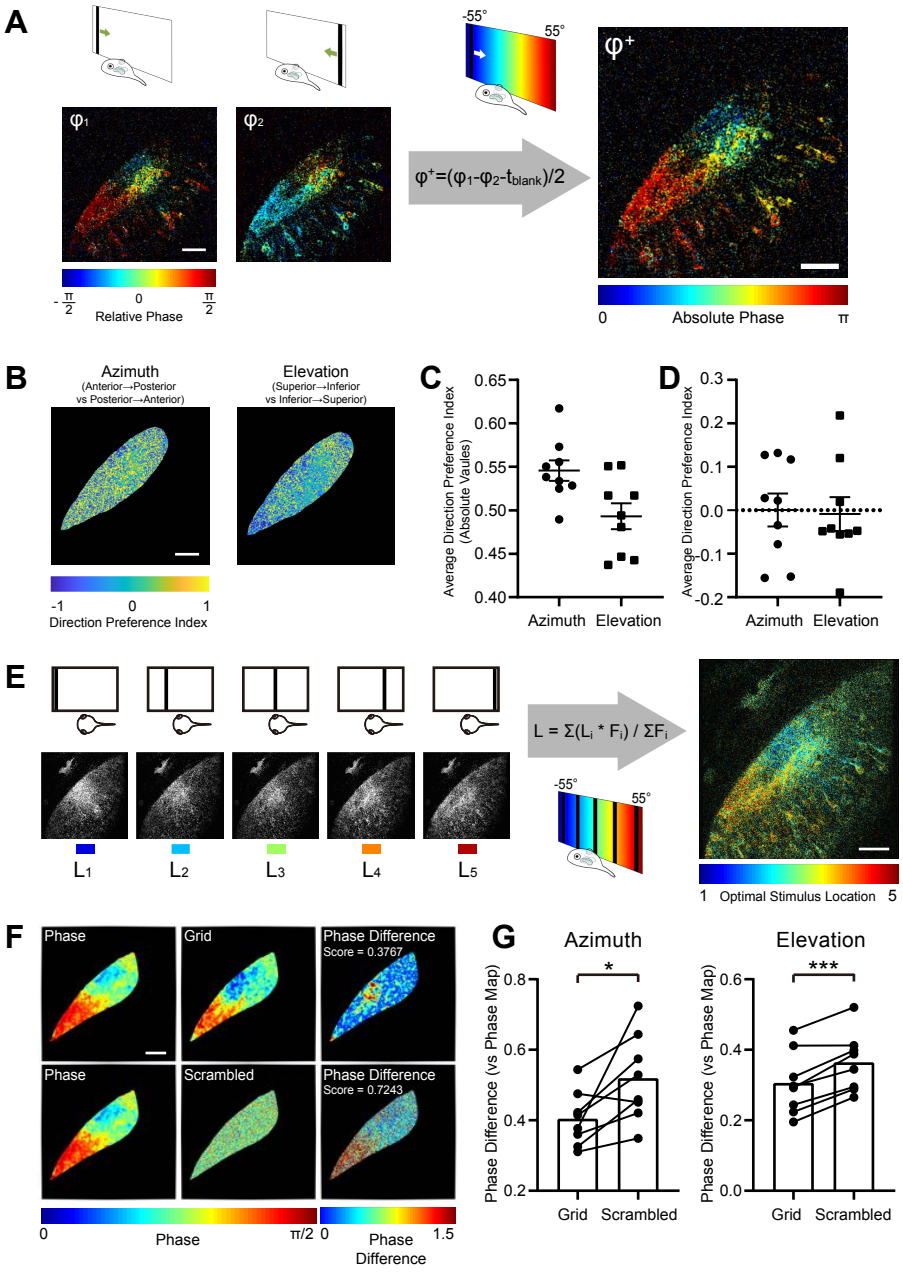

Supplemental Figure S1

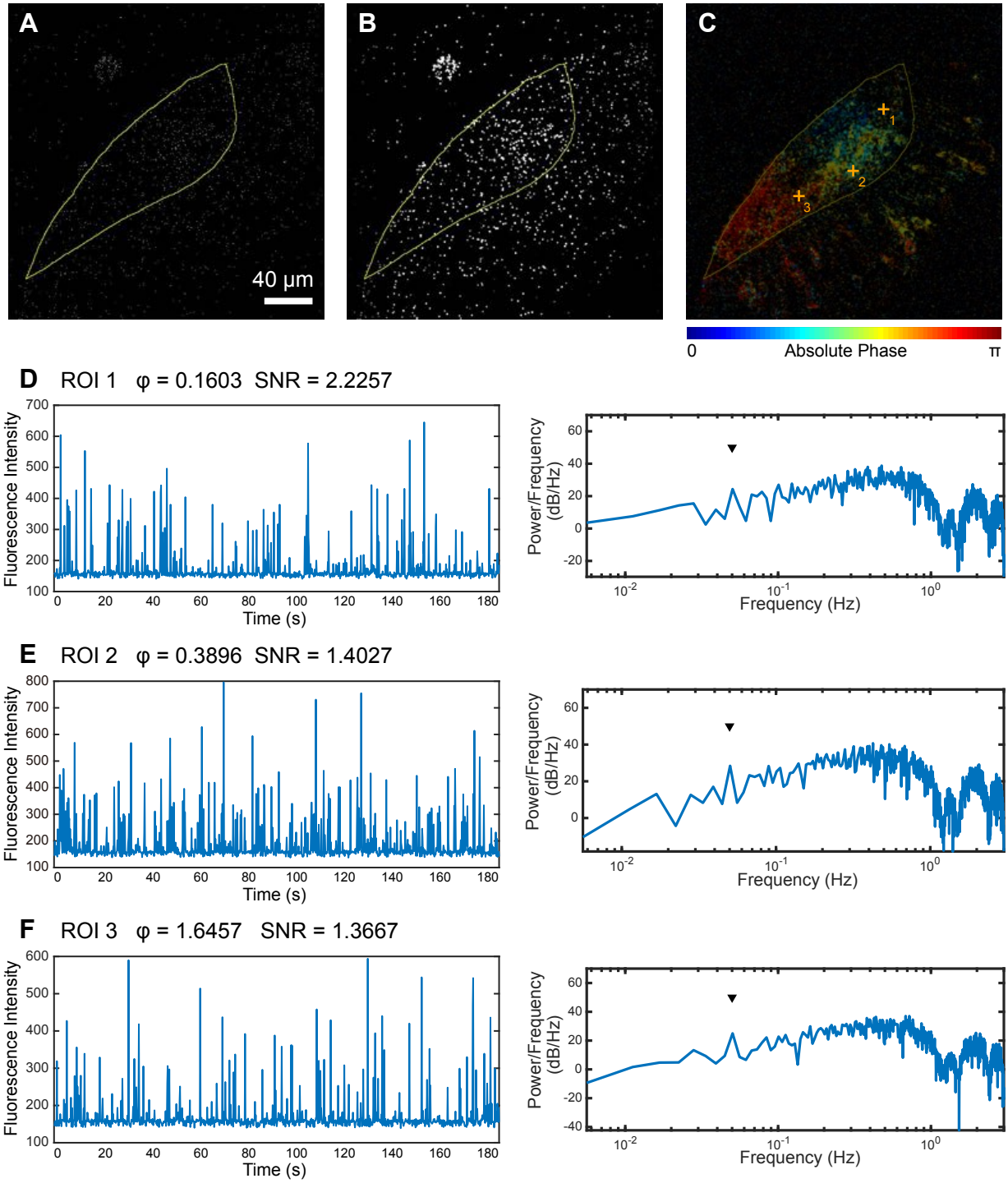

Supplemental Figure S2

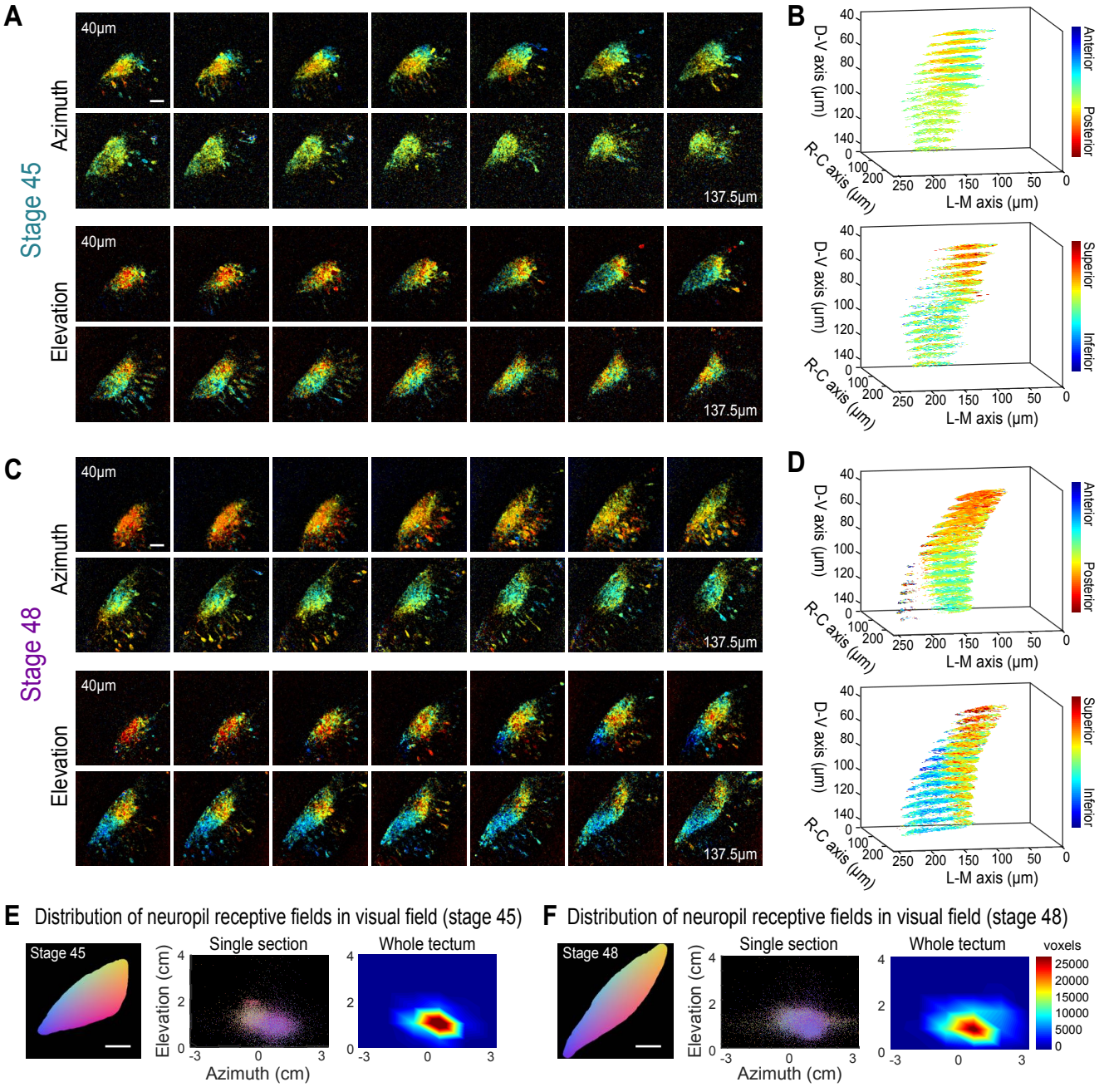

Supplemental Figure S3

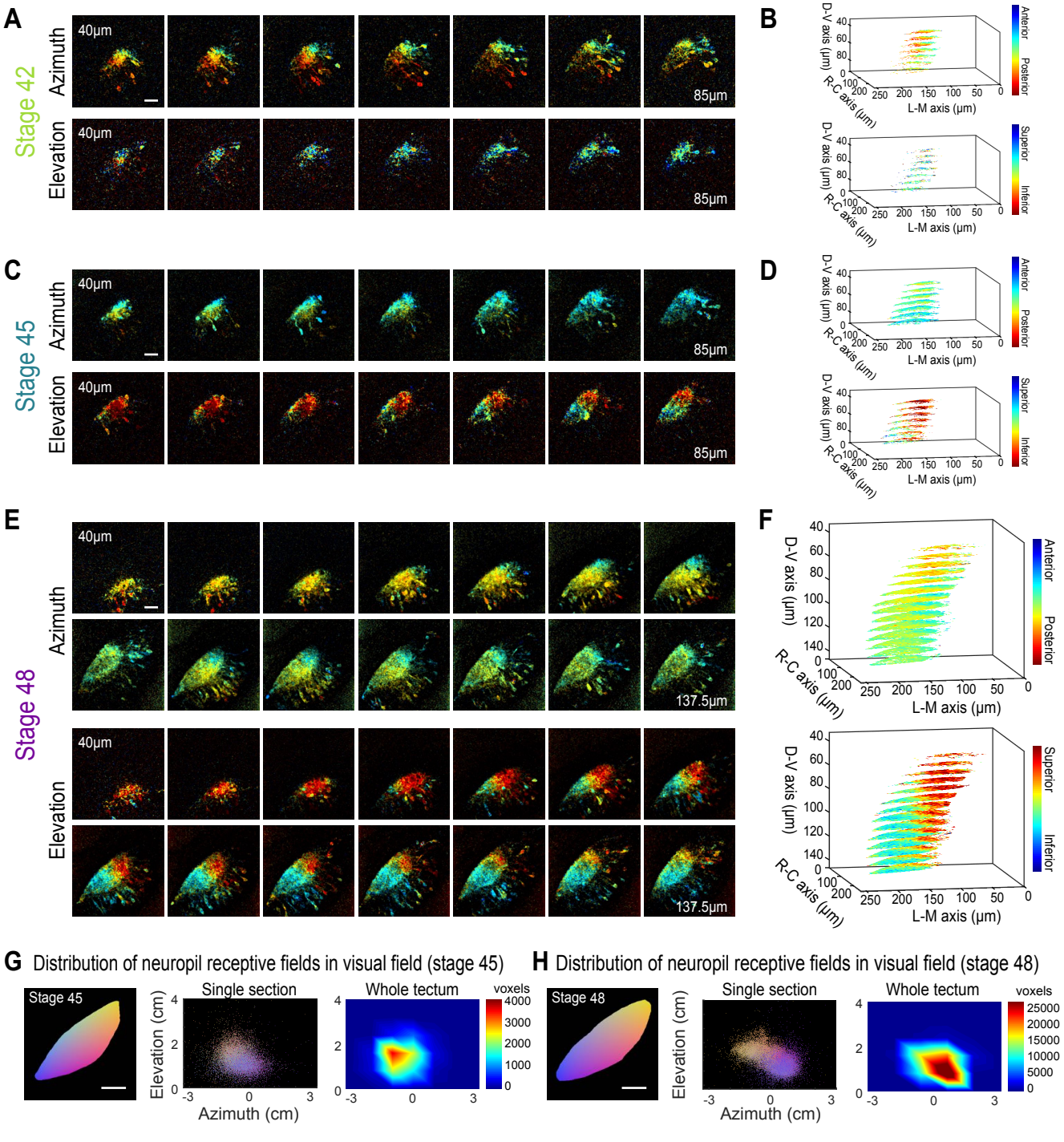

Supplemental Figure S4

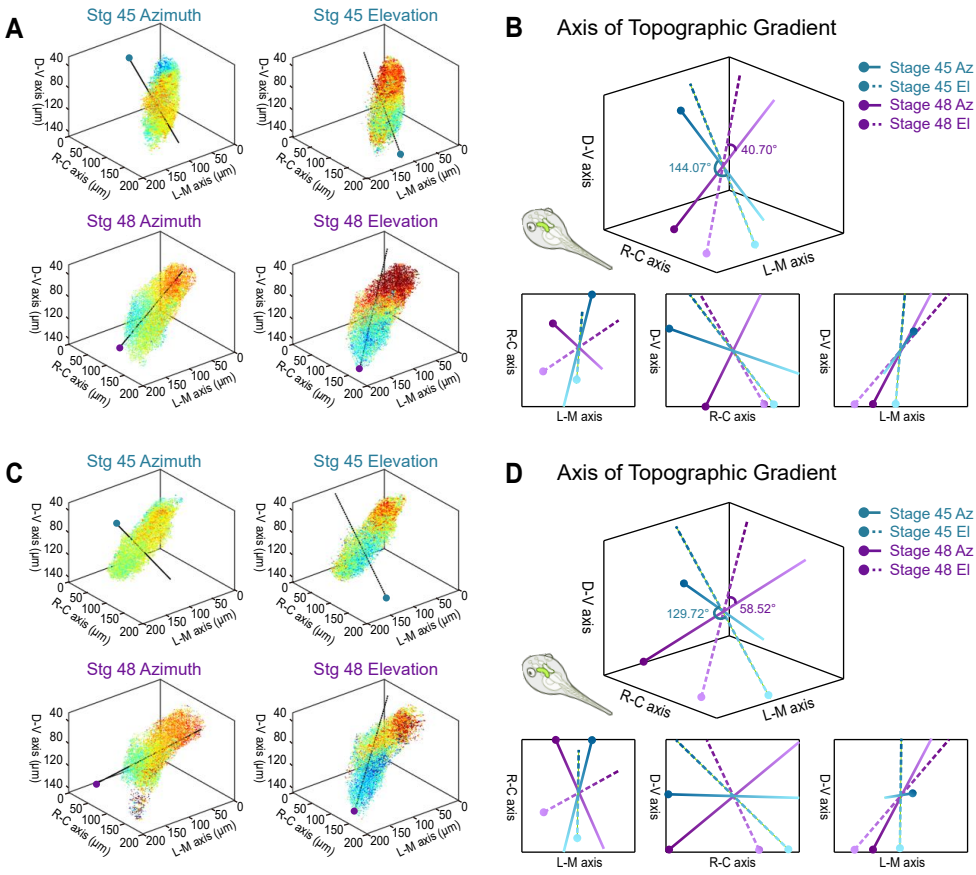

Supplemental Figure S5

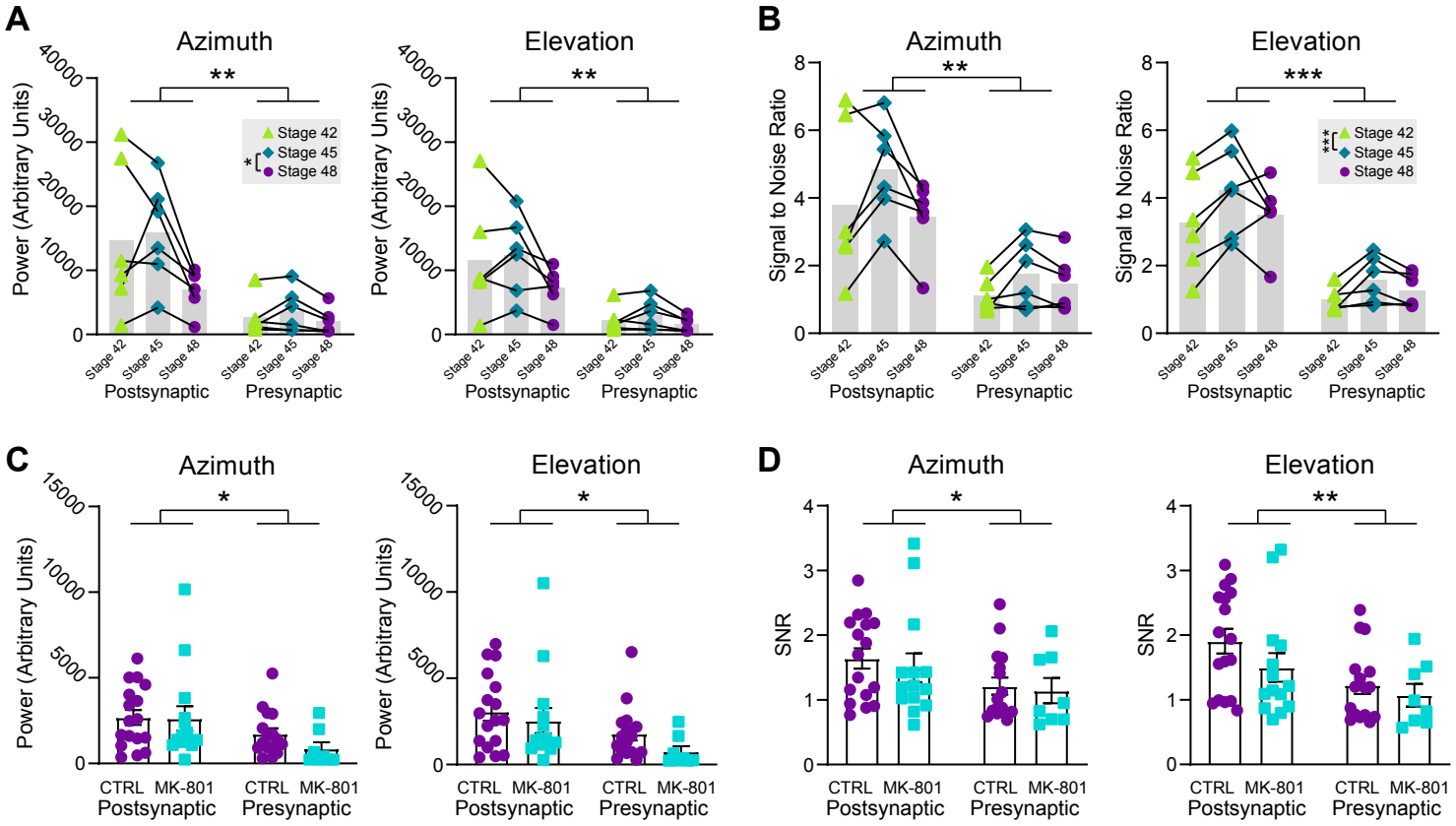

Supplemental Figure S6

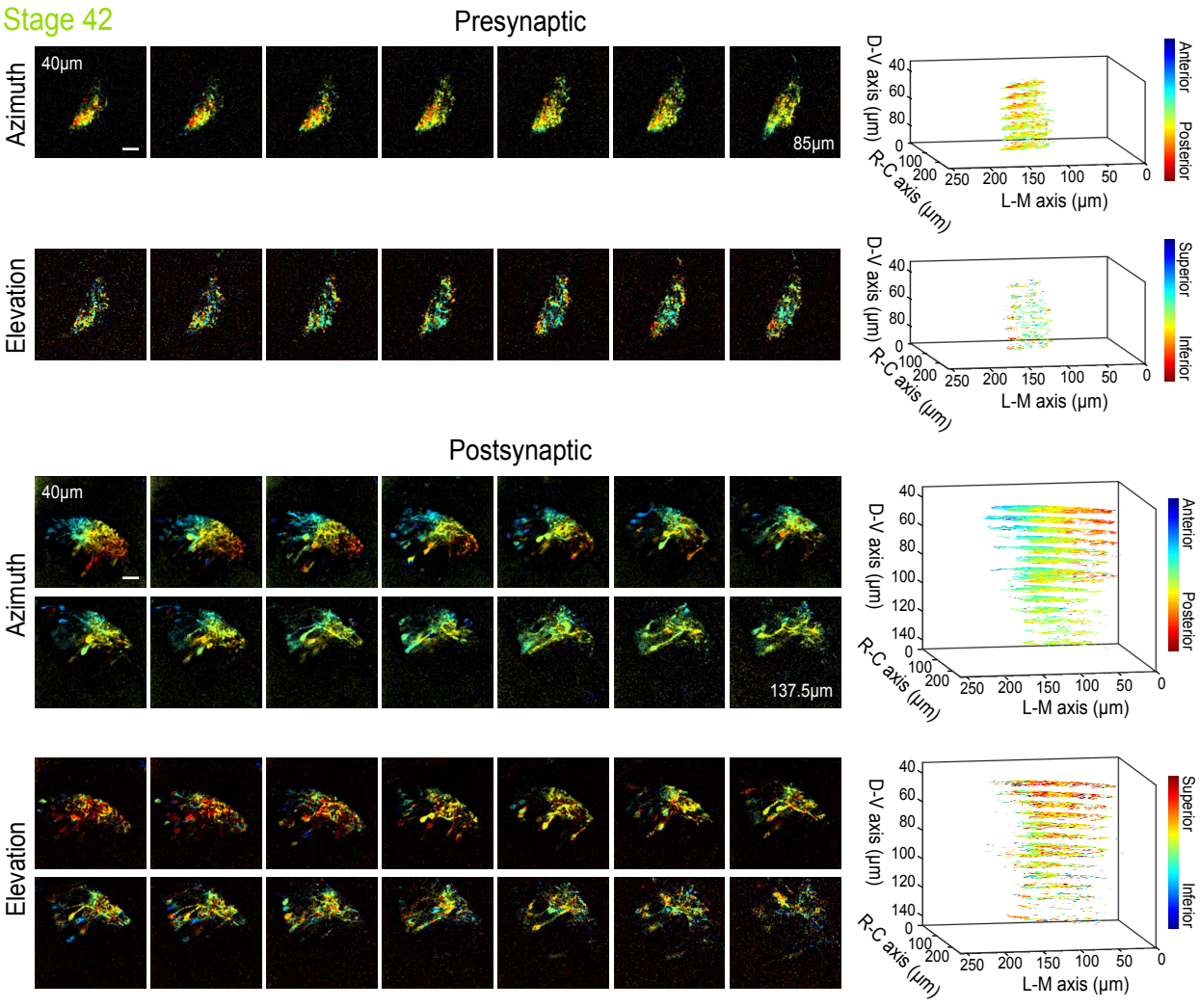

Supplemental Figure S7

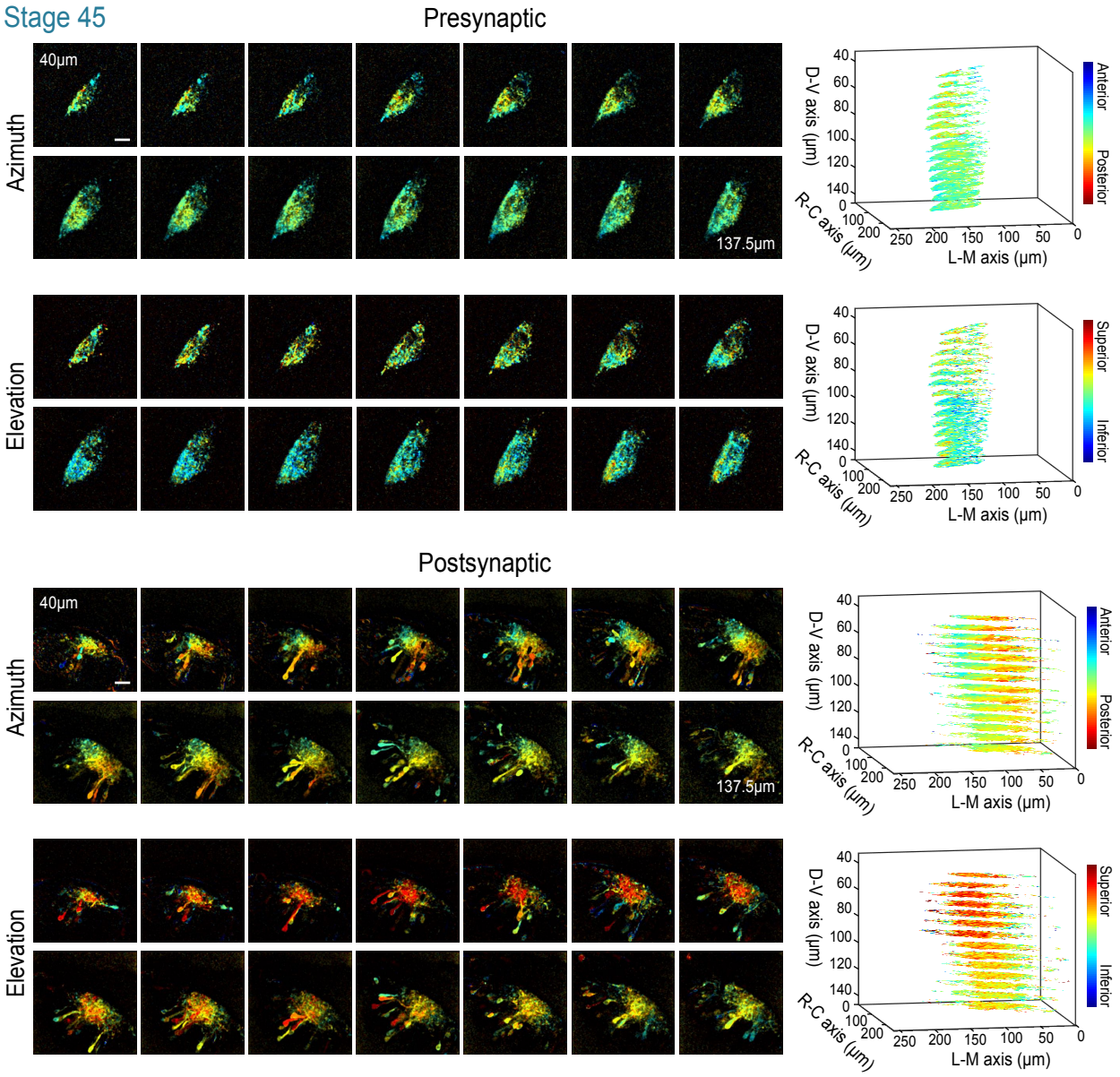

Supplemental Figure S8

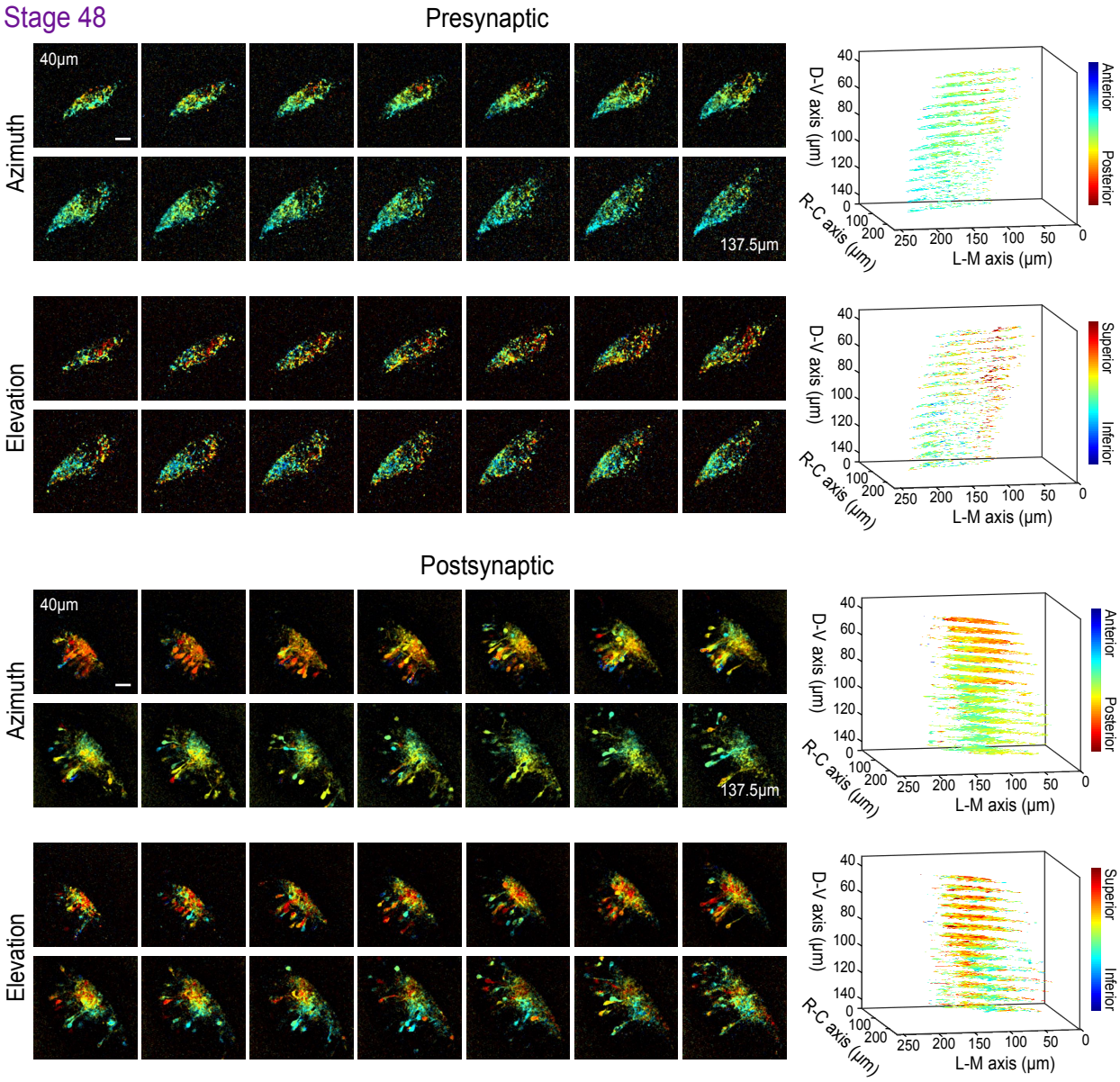

Supplemental Figure S9

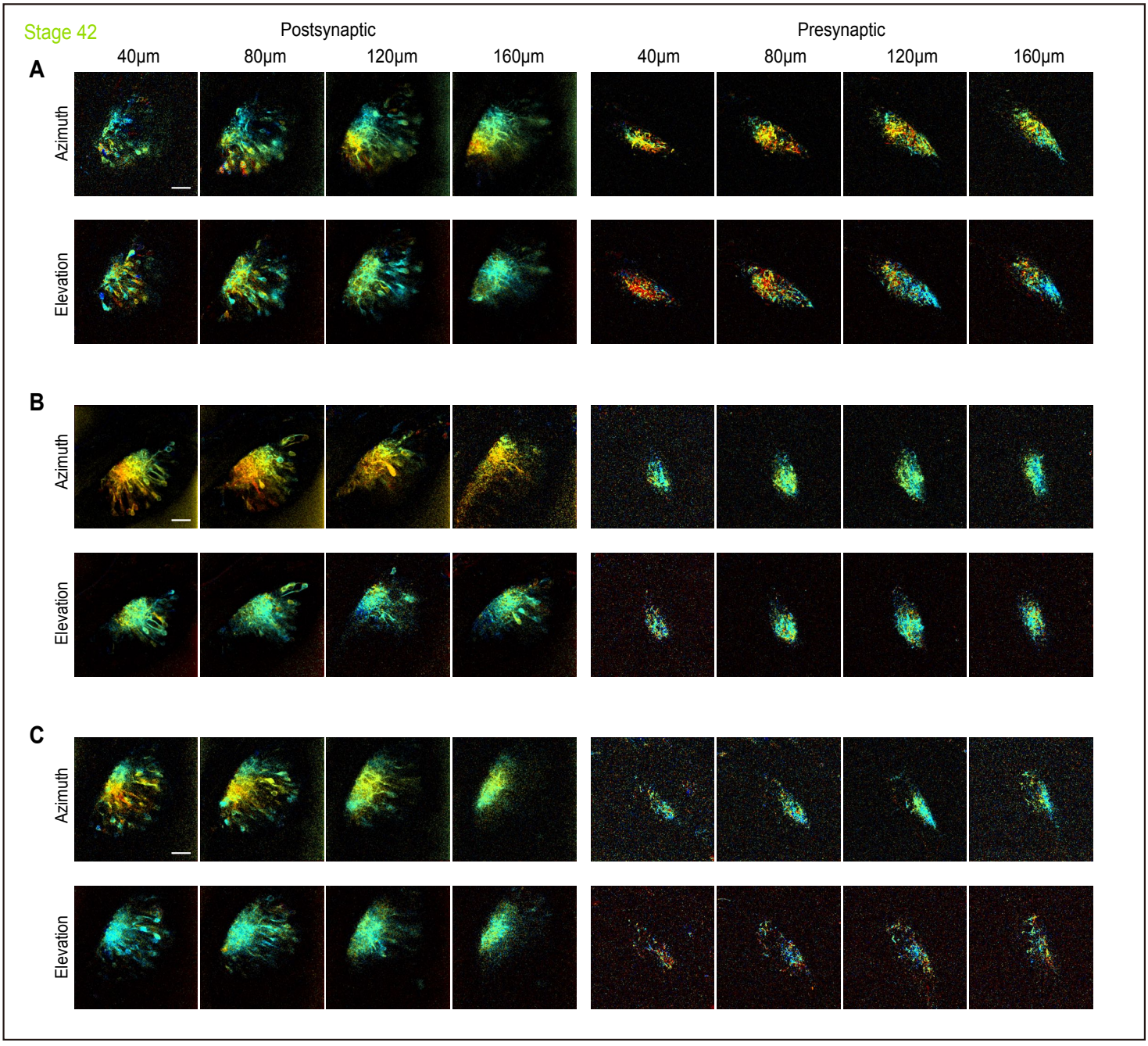

Supplemental Figure S10

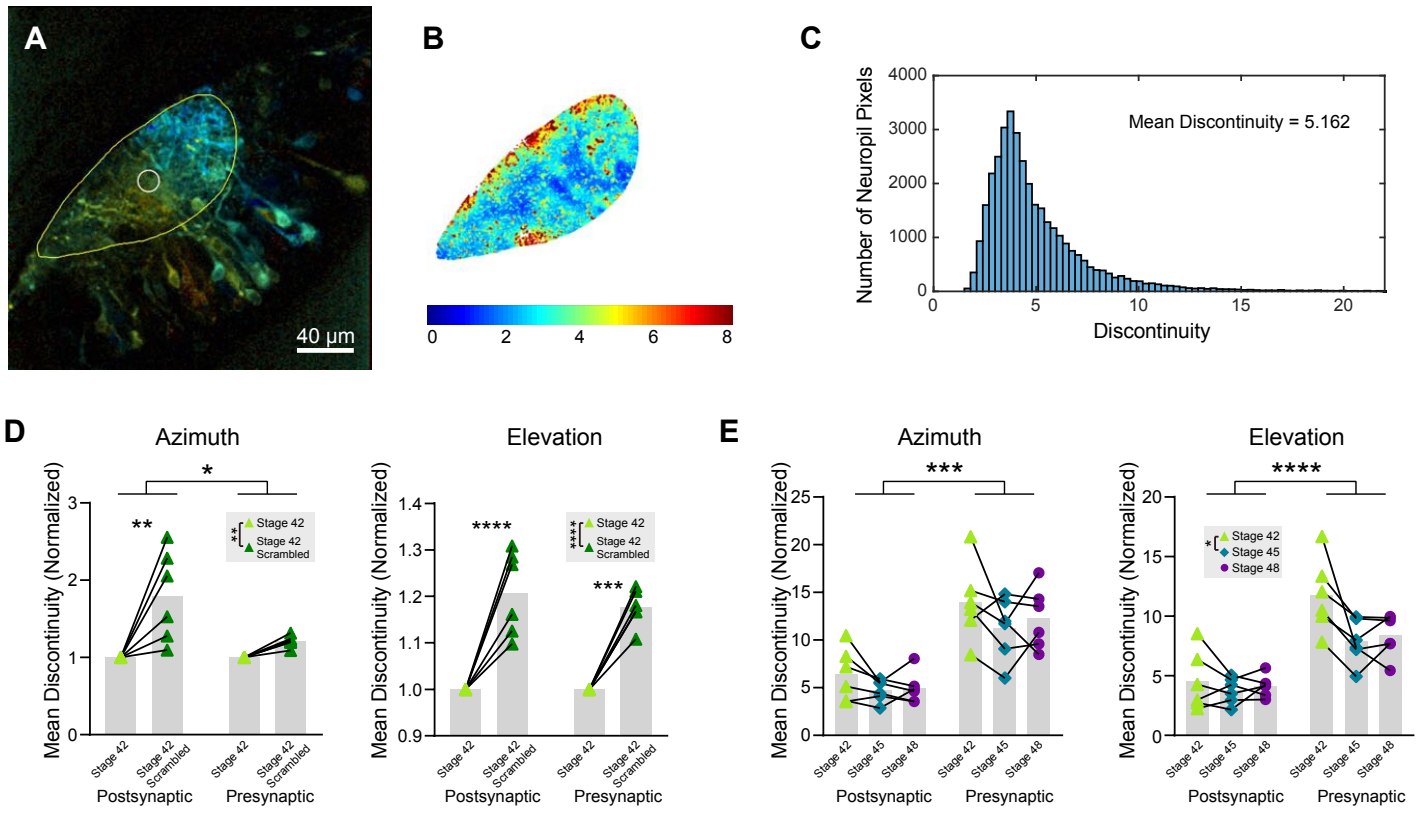

Supplemental Figure S11

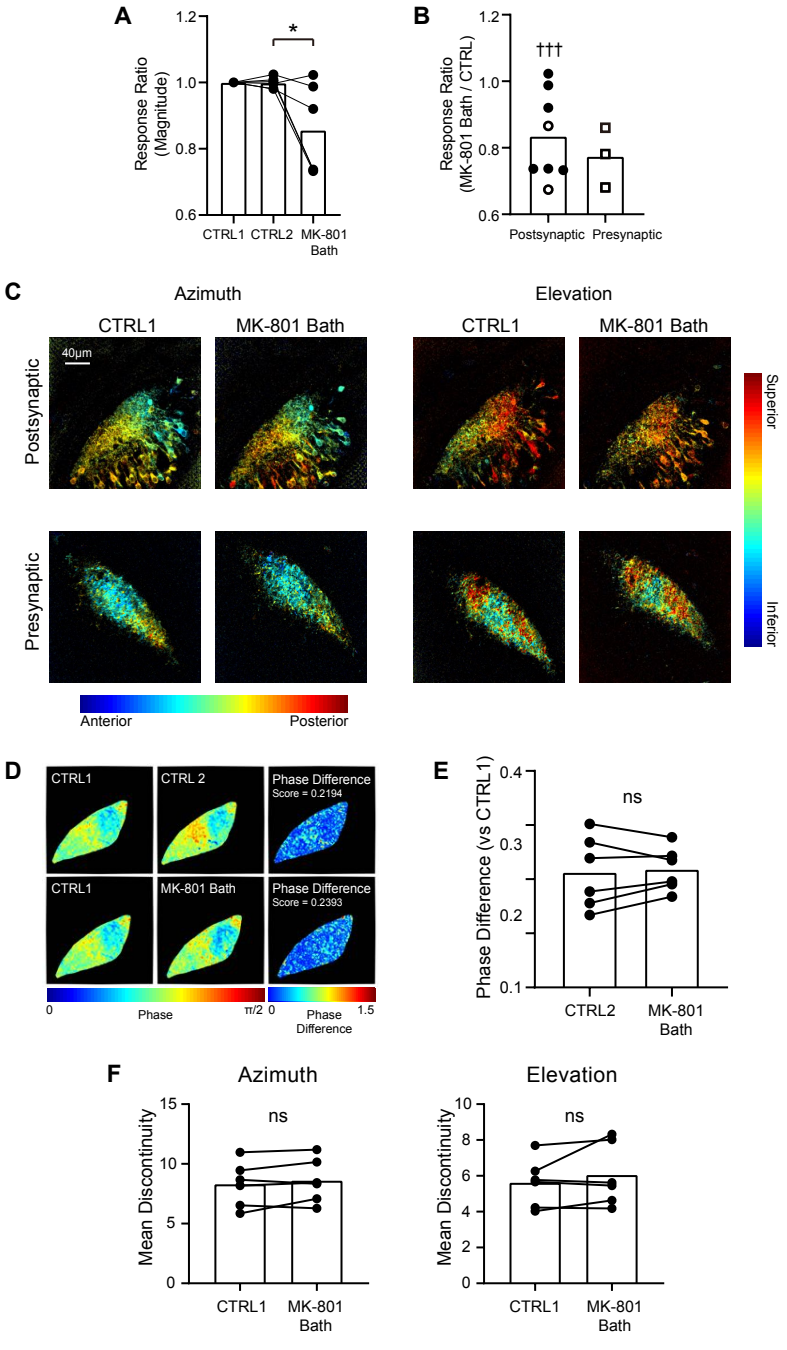

Supplemental Figure S12

Supplementary Information Text

Fig. S1. Tectal response to positioned stimuli and extraction of the retinotopic map.
(A) Calculating phase maps from responses to drifting bar stimuli (azimuth). Absolute phase (φ_+) was calculated by taking the difference of phase maps extracted from opposite direction drifting bars (φ_1 and φ_2). t_{blank} represents the fixed interval between each bar sweep.

(B) Pixelwise direction preference index values in an example animal. Direction preference index is calculated as the difference between the Fourier power at the stimulation frequency for the responses evoked by opposite direction drifting bars, divided by their sum. While each pixel shows a preference for one of the two directions, pixel-wise direction preference is evenly distributed throughout the tectal neuropil.

(C) Absolute values of pixelwise direction preference index averaged over the tectal neuropil (n = 9 transgenic animals).

(D) Pixelwise direction preference index averaged over the tectal neuropil. The average direction preference indices do not significantly differ from 0 for either azimuth or elevation, indicating no overall direction preference in the neuropil (n = 9 transgenic animals, n.s. by one-sample t-test).

(E) Calculating grid maps from average tectal response to each stimulus position. Each pixel is assigned an “optimal stimulus position” as a number between 1 to 5 based on the pixel’s $\Delta F/F_0$ responses to all 5 stimulus positions, which gives an estimate of the location of the pixel’s receptive field center.

(F) Comparing phase and grid maps extracted from the same animal. A Gaussian filter with $\sigma = 3$ was applied to both the phase and grid maps, optimal stimulus position values in grid maps were converted to equivalent phase values, the two maps were aligned based on time average images, then differences between phase values in the two maps were calculated for each pixel in the neuropil and averaged to obtain a phase difference score. This score was compared to the phase difference score for the phase map compared to a scrambled version of the phase map, in which all phase values in the neuropil region were randomly shuffled.

(G) Phase difference score between phase maps, grid maps and scrambled phase maps. The phase difference score comparing phase and grid maps was significantly smaller than for phase and scrambled phase in both azimuth and elevation maps (n = 8 transgenic animals, paired t-tests, azimuth $t(7) = 2.968$, $^*p = 0.021$; elevation $t(7) = 5.947$, $^{***}p = 0.0006$).

Fig. S2. Pixel-wise analysis for phase mapping

(A) Single frame of raw calcium signal from a single 2-photon optical plane in a 3D volume in a GCaMP6s transgenic tadpole imaged at 6 Hz, responding to an anterior-to-posterior drifting bar (same animal as Fig. 1).

(B) Frame in (A) after application of a Gaussian filter with $\sigma = 1$.

(C) Absolute phase map color coded for response positions in azimuth. Pixel ROIs labelled for 3 sites.

(D) Raw calcium trace and Fourier power spectrum of its first differential at pixel ROI #1. The relative phase at the stimulus frequency is 0.1603.

(E) Raw calcium trace and Fourier power spectrum of its first differential at pixel ROI #2. The relative phase at the stimulus frequency is 0.3896.

(F) Raw calcium trace and Fourier power spectrum of its first differential at pixel ROI #3. The relative phase at the stimulus frequency is 1.6457.

Fig. S3. Retinotopic map in a transgenic tadpole (tadpole #2) at stage 45 and stage 48.

(A) Phase maps extracted from the tadpole at stage 45. Stack of 14 optical sections with 7.5 μm spacing between slices.

(B) Phase maps in A rendered as 3D volume.

(C) Phase maps extracted from the same tadpole at stage 48. Stack of 14 optical sections with

7.5 μm between slices.

(D) Phase maps in C rendered as 3D volume. In B and D, only pixels in the neuropil region with SNR > 1.5 are shown.

(E, F) Distribution of neuropil receptive fields in the visual field at (E) stage 45 and (F) stage 48. Colors represent tectal neuropil coordinates (left, middle). Density plots (right) show distribution of neuropil receptive fields from the whole tectum mapped onto the stimulus display area (summed from 14 optical sections, 7.5 μm between slices).

Fig. S4. Retinotopic map in a transgenic tadpole (tadpole #3) at stage 42, 45 and stage 48.

(A) Phase maps extracted from the tadpole at stage 42. Stack of 7 optical sections, 7.5 μm between slices.

(B) Phase maps in A rendered in 3D volume.
(C) Phase maps extracted from the same tadpole at stage 45. Stack of 7 optical sections, 7.5 μm between slices.
(D) Phase maps in C rendered in 3D volume.
(E) Phase maps extracted from the same tadpole at stage 48. Stack of 14 optical sections, 7.5 μm between slices.
(F) Phase maps in E rendered in 3D volume. In B, D and F, only pixels in the neuropil region with SNR > 1.5 are shown.
(G-H) Distribution of neuropil receptive fields in the visual field at (E) stage 45 and (F) stage 48. Colors represent tectal neuropil coordinates (left, middle). Density plots (right) show distribution of neuropil receptive fields from the whole tectum mapped onto the stimulus display area (summed from 7 optical sections at stage 45 and 14 sections at stage 48, 7.5 μm between slices).

Fig. S5. Developmental shifting of the topographic gradients at stage 45 and stage 48.

(A) 3D axes of topographic gradients at stage 45 and 48 in a transgenic tadpole (same animal as in Fig. 2). Phase maps were constructed from 14 optical sections at 7.5 μm intervals. For each optical section, 1000 random pixels in the neuropil region with SNR > 1.5 were plotted as 3D scatter points, with color indicating phase (same scales as in Fig. 2E,G). A black line in each 3D volume indicates the direction of the mean topographic (phase) gradient. The dot at the end of each line indicates the anterior direction for azimuth and inferior direction for elevation.
(B) Comparison of topographic gradient axes at stage 45 vs 48 in same animal.
(C) 3D axes of topographic gradient at stage 45 and 48 in a transgenic tadpole (same animal as in Fig. S2). Phase maps are shown in same manner as panel A.
(D) Comparison of topographic gradient axes at stage 45 vs 48, calculated from the phase maps shown in panel C.

Fig. S6. Comparison of signal strength and SNR at different developmental stages

(A) Fourier power at the stimulus frequency in response to drifting bar stimuli for GCaMP6s hemimosaic tadpoles at stages 42, 45 and 48 (n = 6 animals). Azimuth measurements were made presenting anterior-to-posterior drifting bars, and elevation with inferior to superior drifting bars. The power is calculated for pixel-wise calcium traces and averaged

over the neuropil. Two-way mixed measures ANOVA for stage vs pre/post compartment showed a significant main effect for compartment in both the azimuth and elevation axes. The main effect for stages was significant in the azimuth axis. Azimuth: $F_{compartment}$ (1, 10) = 10.23, **p = 0.0095; F_{stages} (1.362, 13.62) = 5.013 with Greenhouse-Geisser correction, *p = 0.0335. Elevation: $F_{compartment}$ (1, 10) = 11.56, **p = 0.0068; Post-hoc Tukey tests for stages in the azimuth axis showed a significant difference between stage 45 and 48, q(11) = 4.655, *p = 0.0181.

(B) Signal-to-noise ratio for the same tadpoles, calculated pixel-wise and averaged over the neuropil. Two-way mixed measures ANOVA for stage vs pre/post compartment showed a significant main effect for compartment in both the azimuth and elevation axes. The main effect for stages was significant in the elevation axis. Azimuth: $F_{compartment}$ (1, 10) = 14.88, **p = 0.0032. Elevation: $F_{compartment}$ (1, 10) = 21.47, ***p = 0.0009; F_{stages} (1.370, 13.70) = 6.402 with Greenhouse-Geisser correction, *p = 0.0175. Post-hoc Tukey tests for stages in the elevation axis showed a significant difference between stage 42 and 45, q(11) = 8.197, ***p = 0.0003.

(C) Fourier power at the stimulus frequency for control and MK-801-reared mRNA tadpoles imaged post- or presynaptically at stage 48. (Postsynaptic: CTRL n = 17, MK-801 n = 14; Presynaptic: CTRL n = 16, MK-801 n = 8.) Two-way independent measures ANOVA for drug vs compartment shows significant main effects for compartment, for both the azimuth and elevation axes. Azimuth: $F_{compartment}$ (1, 51) = 6.684, *p = 0.0126; Elevation: $F_{compartment}$ (1, 51) = 6.992, *p = 0.0109.

(D) Signal-to-noise ratio for the same tadpoles in (E), calculated pixel-wise and averaged over the neuropil. Two-way independent measures ANOVA for drug vs compartment shows significant main effects for compartment, for both the azimuth and elevation axes. Azimuth: $F_{compartment}$ (1, 51) = 4.446, *p = 0.0399; Elevation: $F_{compartment}$ (1, 51) = 7.856, **p = 0.0071.

Fig. S7. Phase maps extracted from a GCaMP6s mRNA hemimosaic tadpole at stage 42. The animal expressed GCaMP presynaptically in the left tectum, and postsynaptically in the right tectum. The maps were extracted using 36°-wide instead of 18°-wide drifting bars.

Scale bars are 40μm.

Fig. S8. **Phase maps extracted from a GCaMP6s mRNA hemimosaic tadpole at stage 45** Pre- and postsynaptic phase maps were extracted from the same animal as in Fig. S7 at stage 45. The maps were extracted using 18°-wide drifting bars.
Scale bars are 40μm.

Fig. S9. Phase maps extracted from a GCaMP6s mRNA hemimosaic tadpole at stage 48 Pre- and postsynaptic phase maps extracted from the same animal as in Figs. S7 and S8 at stage 48. The maps were extracted using 18°-wide drifting bars.
Scale bars are 40μm.

Fig. S10. Example phase maps from three GCaMP6s mRNA hemimosaic tadpoles imaged at stage 42. Stacks of 4 optical sections from 40 μm to 160 μm below the surface with 40 μm spacing between slices. For each panel (A, B, C), postsynaptic (left) and presynaptic (right) maps for the azimuth (top) and elevation (bottom) axes were collected in the same animals.
Scale bars are 40μm.

Fig. S11. Characterization of mean local discontinuity measurements.
(A) Example azimuth phase map for a stage 48 GCaMP6s mRNA tadpole (postsynaptic labelling). Pixel brightness indicates SNR. Yellow outline defines the neuropil area. White outline shows the 15-pixel (7.44 μm) radius region evaluated around a sample pixel.
(B) Scatterplot of neuropil local discontinuity values from the phase map in (A). Dark red corresponds to values greater than 8.
(C) Histogram of the discontinuity values in (B).
(D) Normalized mean discontinuity in stage 42 tadpole maps (same data as in (D)) compared to their scrambled versions (where phase values at different neuropil coordinates were randomly shuffled). Measured discontinuity values were normalized by dividing by mean discontinuity in the original map. Two-way repeated measures ANOVA for shuffling vs compartment showed a significant interaction and significant main effects for both shuffling and compartment for azimuth; and a significant main effect for shuffling for elevation. (n=6) Azimuth: $F_{interaction}(1,10) = 5.955$, *p = 0.0348; $F_{shuffling}(1,10) = 17.60$, **p = 0.0018; $F_{compartment}(1, 10) = 5.955$, *p = 0.0348; Elevation: $F_{shuffling}(1,10) = 90.49$, ****p < 0.0001. Post-hoc t-tests with Sidak correction showed stage 42 discontinuity was

significantly lower in original maps compared to scrambled in postsynaptic maps in the azimuth axis; and both pre- and postsynaptic maps in the elevation axis. Azimuth: postsynaptic $t(10) = 4.692$, $^{**}p = 0.0017$; Elevation: postsynaptic $t(10) = 7.286$, $^{****}p < 0.0001$; presynaptic $t(10) = 6.167$, $^{***}p = 0.0002$.

(E) Tectal neuropil area-normalized mean discontinuity in tadpoles at stages 42, 45 and 48. The radius of the region evaluated around each pixel was normalized between stages in proportion to the area of the neuropil. Two-way mixed measures ANOVA for stage vs compartment showed significant main effects for compartment in both azimuth and elevation axes, and a significant main effect for stage for elevation. (n=6) Azimuth: $F_{compartment}$ (1, 10) = 34.27, $^{***}p = 0.0002$; Elevation: $F_{compartment}$ (1, 10) = 39.55, $^{****}p < 0.0001$; F_{stages} (1.175, 11.75) = 6.134 with Greenhouse-Geisser correction, $^{*}p = 0.0257$. Post-hoc Tukey tests showed a significant difference in discontinuity in the elevation axis between stages 42 and 45, $q(11) = 4.180$, $^{*}p = 0.0323$.

Fig. S12. Tectal response to drifting bar stimuli after acute MK-801 application.

(A) Two sets of control phase maps were collected approximately 30 min apart, followed by application of MK-801 in the imaging chamber to achieve a final concentration of 10 μM. The Fourier power at the stimulation frequency for the 3 conditions were normalized by dividing all values by the CTRL1 measurement. Paired t-test showed a significant difference between CTRL2 and MK-801 bath ($n = 6$, $t(5) = 2.616$, $^{*}p = 0.0471$), corresponding to a 14% decrease in response magnitude following acute MK-801 application.

(B) The fractional decrease of Fourier power at the stimulation frequency in response to an anterior to posterior drifting bar after MK-801 bath application was measured for pre- and postsynaptic neuropil. Filled data points indicate data from panel (A); unfilled data points indicate data from additional animals measured without a second control recording. One-sample t-test showed a significant response magnitude decrease after MK-801 bath application in the postsynaptic neuropil ($n = 8$, $t(7) = 4.171$, $^{\dagger\dagger\dagger}p = 0.0042$).

(C) Maps extracted from drifting bar experiments before and after acute MK-801 application reveal the robustness of phase mapping to the effects of MK-801 treatment. Phase maps in each row were extracted from the same animal.

(D) Quantifying the difference between azimuth phase maps from drifting bar experiments before and after acute MK-801 application. The phase maps from CTRL2 or acute MK-

801 treatment were subtracted from CTRL1 baseline maps, and the resulting phase difference maps were averaged over the neuropil to obtain a phase difference score.
(E) Phase difference scores (versus CTRL1) for azimuth phase maps were used to compare CTRL2 vs MK-801 conditions. A paired t-test showed no significance ($n = 6$, $t(5) = 0.4812$, $p = 0.651$), indicating the maps were not different between these conditions.
(F) Tectal neuropil mean discontinuity does not change following acute MK-801 bath application. ($n = 6$, azimuth $t(5) = 1.271$, $p=0.2598$; elevation $t(5) = 1.232$, $p=0.2727$, paired t-tests).

Table S1. 3D axis gradient vectors and their angles with respect to cardinal axes

		3D Gradient Vectors			Angle with Cardinal Axes		
		x	y	z	x - mediolateral	y - rostrocaudal	z - dorsoventral
tadpole #1	45 Azimuth	79.12	315.71	147.92	77.21	27.98	65.56
	48 Azimuth	-158.52	151.43	-407.45	69.96	70.90	28.28
	45 Elevation	-8.79	-91.68	-158.66	87.25	60.02	30.13
	48 Elevation	-360.91	-241.00	-557.04	59.26	70.04	37.92
tadpole #2	45 Azimuth	44.45	187.01	10.17	76.65	13.70	86.97
	48 Azimuth	-92.36	215.07	-233.99	73.80	49.47	45.01
	45 Elevation	-2.44	-85.10	-110.38	89.00	52.38	37.64
	48 Elevation	-97.91	-53.91	-147.69	58.09	73.08	37.12

Table S1 - 3D axis gradient vectors and their angles with respect to cardinal axes.
3D azimuth and elevation gradient vectors for the data shown in Fig. S5, and their angles with respect to the cardinal axes (in degrees).

Movie S1 (separate file). Tectum calcium response to drifting bars.
Example of calcium responses to one cycle of opposite direction drifting bars (left: anterior to posterior; right: posterior to anterior). Images were acquired at 6 Hz (total 20 seconds), then a time average projection was taken for every 10 frames. The clip is looped once for better visibility of calcium response patterns.

Movie S2 (separate file). 3D azimuth phase maps of a transgenic tadpole at stage 45 and stage 48
Rotated views of the 3D azimuth phase map shown in Fig. 2E (left) and Fig. 2G (right).

Movie S3 (separate file). 3D elevation phase maps of a transgenic tadpole at stage 45 and stage 48
Rotated views of the 3D elevation phase maps shown in Fig. 2E (left) and Fig 2G. (right).

Movie S4 (separate file). 3D azimuth phase maps of a transgenic tadpole (tadpole #2) at stage 45 and stage 48
Rotated views of the 3D azimuth phase maps shown in Fig. S3B (left) and Fig. S3D (right).

Movie S5 (separate file). 3D azimuth phase maps of a transgenic tadpole (tadpole #2) at stage 45 and 48
Rotated views of the 3D elevation phase maps shown in Fig. S3B (left) and Fig. S3D (right).

Movie S6 (separate file). Presynaptic 3D azimuth phase maps of a GCaMP6s mRNA hemimosaic tadpole at stage 42, 45 and 48
Rotated views of the presynaptic 3D azimuth phase maps shown in Fig. S7 (left) S8 (middle) and S9 (right).

Movie S7 (separate file). Presynaptic 3D elevation phase maps of a GCaMP6s mRNA hemimosaic tadpole at stage 42, 45 and 48
Rotated views of the presynaptic 3D elevation phase maps shown in Fig. S7 (left) S8 (middle) and S9 (right).

Movie S8 (separate file). Postsynaptic 3D azimuth phase maps of a GCaMP6s mRNA hemimosaic tadpole at stage 42, 45 and 48

Rotated views of the postsynaptic 3D azimuth phase maps shown in Fig. S7 (left) S8 (middle) and S9 (right).

Movie S9 (separate file). Postsynaptic 3D elevation phase maps of a GCaMP6s mRNA hemimosaic tadpole at stage 42, 45 and 48

Rotated views of the postsynaptic 3D elevation phase maps shown in Fig. S7 (left) S8 (middle) and S9 (right).

Dataset S1 (separate file). Data plotted in Figure 4C

Mean discontinuity values in tadpoles at stages 42, 45 and 48 for azimuth and elevation maps of presynaptic axonal inputs and postsynaptic tectal dendritic arbors in the neuropil.

Dataset S2 (separate file). Data plotted in Figure 4F

Tab 1: Receptive field sharpness measures along the azimuth visual axis for tectal neuron somata at stages 42, 45 and 48

Tab 2: Receptive field sharpness measures along the elevation visual axis for tectal neuron somata at stages 42, 45 and 48

Dataset S3 (separate file). Data plotted in Figure 5B

Mean discontinuity values in control and MK-801-reared tadpoles, for the presynaptic (RGC axon terminals) and postsynaptic (tectal dendritic neuropil) compartments, measured independently for the azimuth and elevation axes.

Dataset S4 (separate file). Data plotted in Figure 5C

Tab 1: Receptive field sharpness measures along the azimuth visual axis for tectal neuron somata at stage 48 under control or MK-801-rearing conditions.

Tab 2: Receptive field sharpness measures along the elevation visual axis for tectal neuron somata at stage 48 under control or MK-801-rearing conditions.

Dataset S5 (separate file). Data plotted in S1 Figs C, D and G

Absolute values of pixelwise direction preference index averaged over the tectal neuropil.

Pixelwise direction preference index averaged over the tectal neuropil.

Comparison of phase and grid maps extracted from same animal.

Dataset S6 (separate file). Data plotted in S6 Figs A-D

Signal power for measurements made in hemimosaic tadpoles at stages 42, 45 and 48.

Signal-to-noise ratio for measurements made in hemimosaic tadpoles at stages 42, 45 and 48.

Signal power for measurements made in control and MK-801-reared tadpoles at stage 48.

Signal-to-noise ratio for measurements made in control and MK-801-reared tadpoles at stage 48.

Dataset S7 (separate file). Data plotted in S11 Figs D and E

Mean discontinuity in maps from stage 42 animals compared to scrambled versions of those maps. Raw and normalized datasets.

Mean discontinuity values normalized to tectum size.

Dataset S8 (separate file). Data plotted in S12 Figs A, B, E and F

Comparison of the magnitude of the signal strength at the stimulus frequency at two baseline timepoints and following acute MK-801 application. Data normalized to first baseline measurement.

Signal strength after MK-801 application relative to baseline signal for GCaMP6s expression in postsynaptic and presynaptic compartments.

Mean difference in pixelwise phase (receptive field position) compared to a baseline measurement, showing that acute MK-801-treatment does not significantly alter the map layout.

Measurements of mean local discontinuity in the same animals before and after application of MK-801 in the bath.